END
DATE
FILMED
5-81
DTIC

MICROCOPY RESOLUTION TEST CHART

LEVEL II

(12)

AD A097523

Earth Limb Radiance Transformation

Prepared by S. J. YOUNG
Chemistry and Physics Laboratory
Laboratory Operations
The Aerospace Corporation
El Segundo, Calif. 90245

DTIC
S ELECTE D
APR 0 9 1981
F

2 March 1981

Interim Report

81 4 9 103

This interim report was submitted by The Aerospace Corporation, El Segundo, CA 90245, under Contract No. F04701-80-C-0081 with the Space Division, Deputy for Technology, P. O. Box 92960, Worldway Postal Center, Los Angeles, CA 90009. It was reviewed and approved for The Aerospace Corporation by M. T. Weiss, Vice President and General Manager, Laboratory Operations. Major George A. Kuck, SD/YLXT, was the project officer for the Mission Oriented Investigation and Experimentation Program.
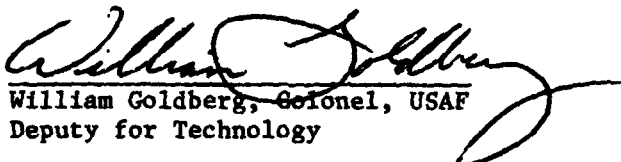
This report has been reviewed by the Public Affairs Office (PAS) and is releasable to the National Technical Information Service (NTIS). At NTIS, it will be available to the general public, including foreign nations.

This technical report has been reviewed and is approved for publication. Publication of this report does not constitute Air Force approval of the report's findings or conclusions. It is published only for the exchange and stimulation of ideas.

George A. Kuck, Major, USAF
Project Officer

Florian P. Meinhardt, Lt Col, USAF
Director of Advanced Space Development

FOR THE COMMANDER

William Goldberg, Colonel, USAF
Deputy for Technology

SECURITY CLASSIFICATION OF THIS PAGE (When Data Entered)

REPORT DOCUMENTATION PAGE		READ INSTRUCTIONS BEFORE COMPLETING FORM
1. REPORT NUMBER SD-TR-81-19	2. GOVT ACCESSION NO. AD-A097523	3. RECIPIENT'S CATALOG NUMBER
4. TITLE (and Subtitle) Earth Limb Radiance Transformation.		5. TYPE OF REPORT & PERIOD COVERED Interim
		6. PERFORMING ORG. REPORT NUMBER TR-0081(6970-04)-1
7. AUTHOR(s) Stephen J. Young		8. CONTRACT OR GRANT NUMBER(s) F04701-80-C-0081
9. PERFORMING ORGANIZATION NAME AND ADDRESS The Aerospace Corporation El Segundo, Calif. 90245		10. PROGRAM ELEMENT, PROJECT, TASK AREA & WORK UNIT NUMBERS
11. CONTROLLING OFFICE NAME AND ADDRESS Space Division Air Force Systems Command Los Angeles Air Force Station P.O. Box 92960 Los Angeles, Calif. 90009		12. REPORT DATE 2 March 1981
		13. NUMBER OF PAGES 33
14. MONITORING AGENCY NAME & ADDRESS(if different from Controlling Office)		15. SECURITY CLASS. (of this report) Unclassified
		15a. DECLASSIFICATION/DOWNGRADING SCHEDULE

16. DISTRIBUTION STATEMENT (of this Report)

Approved for public release; distribution unlimited.

17. DISTRIBUTION STATEMENT (of the abstract entered in Block 20, if different from Report)

18. SUPPLEMENTARY NOTES

19. KEY WORDS (Continue on reverse side if necessary and identify by block number)

Atmospheric Radiation
Earth Limb Radiation
Infrared

20. ABSTRACT (Continue on reverse side if necessary and identify by block number)

A mathematical transformation is derived for predicting the upsounding (downwelling) infrared atmospheric radiance from measurements of the earth limb radiance profile. The transformation is derived by writing the equation of radiative transfer for each viewing geometry in terms of the altitude dependent volume emission function $J(r)$ and then eliminating $J(r)$ from the equations to define the upsounding profile directly as a weighted integral over the limb profile. An approximate transformation is derived for the important case in which the limb profile is nearly exponential with tangent height. The transformation method is limited to spectral and altitude regions for which the atmosphere is optically thin. Near the centers of strong molecular absorption bands in the mid- and far-infrared region, this limitation restricts application to altitudes above ~100km.

DD FORM 1473
(FACSIMILE)

SECURITY CLASSIFICATION OF THIS PAGE (When Data Entered)

CONTENTS

FIGURES

TABLES

1. Introduction

Consideration of long wavelength infrared radiation emitted by the terrestrial atmosphere is important in application of remote sounding to the atmosphere, treatment of the heat budget of the planet, and estimation of background signal levels for target detection sensors. Direct modeling of this radiation requires detailed consideration of the altitude distribution of infrared active molecular species, the line shape and structure within absorption bands, and, in the upper atmosphere, the population and loss mechanisms of molecules in various vibrational-rotational levels. A familiar operational computer code for performing such direct radiation calculations is that due to Degges (1974). For many applications, the accuracy of predictions based on models is not sufficient. Actual measured radiation levels are required. On the other hand, such measurements are expensive, difficult to obtain, and often not available for the desired observation geometry. Under certain circumstances it is possible to scale radiation measurements made for one observation geometry to another. Such a scaling transformation is considered in this paper. In particular, the problem addressed is that of determining the downwelling atmospheric radiation incident on an upsounding sensor from the tangent-height profile of earth-limb radiation. The derivation of the transformation is considered in Section 2. An important limitation of the method is that it can be applied only under conditions where the atmosphere is optically thin. Consideration of this limitation is made in Section 3. Example applications of the transformation method are made for the 9.6-μm O_3 and 15-μm CO_2 bands in Section 4.

2. Theoretical Formulation

a. General transformation

The fundamental function describing the radiative characteristics of a gaseous medium such as the atmosphere is the volume emission coefficient J. This function describes the energy (e.g., photons or joules) emitted per unit time per unit volume of atmosphere. In general, J is a function of position in the atmosphere and direction of emission. For the present application, it will be assumed that J is a function only of altitude above the earth's surface (and not of geographic position on the earth's surface) and is isotropic. Also, J is, in general, a spectroscopic parameter. In the present context, it is assumed that J is the mean value in some sensor bandpass. In the development presented here, the spectral resolution of the sensor is immaterial and may range from essentially monochromatic to extremely wide band. Radiation emitted along some line of sight through the atmosphere is determined as an integral of J along the line of sight. The geometries relevant to the present problem are shown in Figs. 1a and 2a. (Note that both altitude and tangent height are measured from earth center. R is the earth radius.) Figure 1a illustrates the tangent viewing geometry for limb scanning; z is the tangent height and $N_L(z)$ is the in-band radiance emitted from the line of sight s at z. Figure 1b is a qualitative representation of the profile of $N_L(z)$; H and H_0 are the upper and lower limb scan bounds. Figure 2a illustrates the upsounding viewing geometry. h is the sensor altitude and θ is the local zenith angle of observation; $N_U(h, \theta)$ is the radiance presented to the sensor. Figure 2b is a qualitative representation of the profile $N_U(h)$ for some fixed θ. The limb scanning and upsounding sensors are assumed to have the same bandpass and fields of view. In terms of the volume emission function, the radiative transfer equations for these two lines of sight are

5

(a)
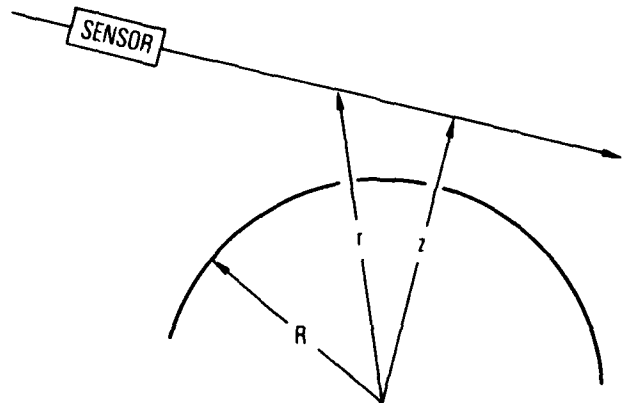
(b)
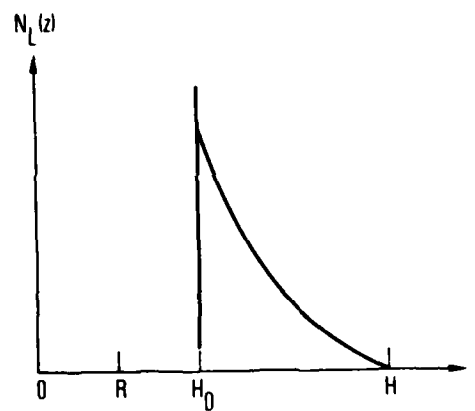

Fig. 1. Limb Scanning Geometry: a) Definition of
Geometry Parameters; b) Qualitative
Tangent Height Radiance Profile

(a)

θ

SENSOR ────────────────→ s

R

h

r

(b)

$N_U(h, \theta)$

0   R H_0 H   →h
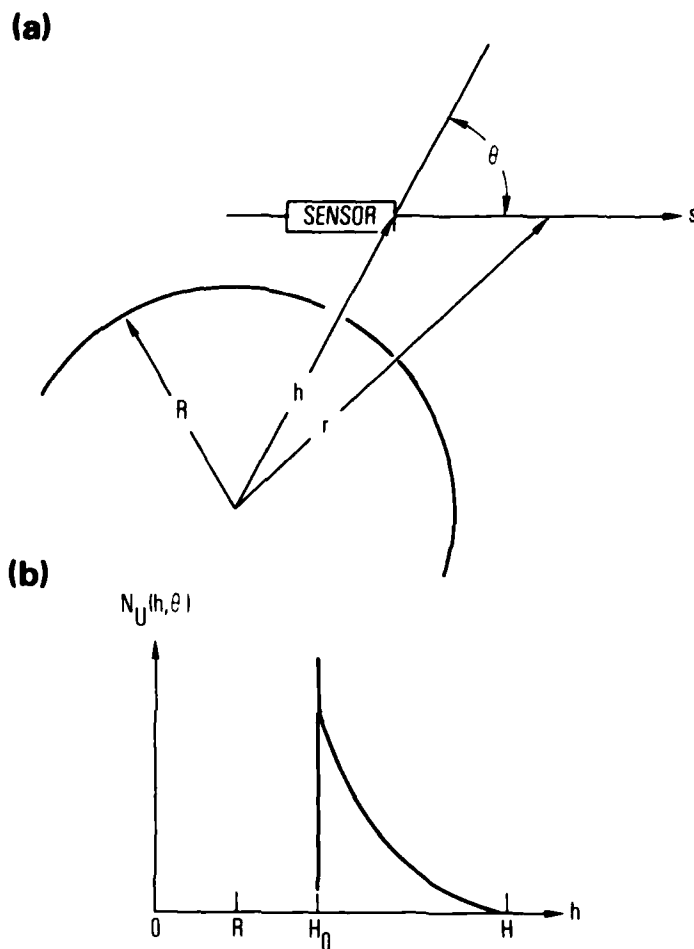
Fig. 2. Upsounding Geometry: a) Definition of
Geometry Parameters; b) Qualitative
Tangent Height Radiance Profile

$$N_L(z) = 2 \int_z^H J(r) \frac{r\,dr}{\left(r^2 - z^2\right)^{\frac{1}{2}}} \qquad (1)$$

and

$$N_U(h, \theta) = \int_h^H J(r) \frac{r\,dr}{\left(r^2 - h^2 \sin^2\theta\right)^{\frac{1}{2}}} \cdot \qquad (2)$$

These equations are well-founded in the general theory of radiative transfer in cylindrical geometry, but are based on three, as yet undiscussed, assumptions. The first is that the fields of view of the two sensors are infinitesimally small. The second is that H is large enough for us to approximate $J(r) = 0$ for $r \geq H$. The third, and most important, is that the radiation processes are occurring in the optically thin regime. This last assumption is treated in Section 3.

Equations (1) and (2) form the basis of the development. The goal is to relate $N_U(h, \theta)$ directly to $N_L(z)$. The method is the elimination of $J(r)$ between (1) and (2). Equation (1) is a form of Abel's integral equation in which $N_L(z)$ is considered as a known function and $J(r)$ is the unknown function. The solution for $J(r)$ is given by the Abel transformation

$$J(r) = -\frac{1}{\pi} \int_r^H \left[\frac{dN_L(z)}{dz} \right] \frac{dz}{\left(z^2 - r^2\right)^{\frac{1}{2}}} \cdot \qquad (3)$$

Substitution of this result into (2) yields

$$N_U(h, \theta) = \int_{r=h}^H \int_{z=r}^H F(r, z)\,dz\,dr \qquad (4)$$

8

where

$$F(r, z) = -\frac{1}{\pi} \frac{dN_L(z)}{dz} \frac{r}{\left(z^2 - r^2\right)^{\frac{1}{2}} \left(r^2 - h^2 \sin^2 \theta\right)^{\frac{1}{2}}} \ . \tag{5}$$

Equation (4) is a simple area integral, and the order of integration over r and z can be interchanged to give the equivalent integral

$$N_U(h, \theta) = \int_{z=h}^{H} \int_{r=h}^{z} F(r, z) \, dr \, dz. \tag{6}$$

Substitution of (5) into (6) yields

$$N_U(h, \theta) = -\frac{1}{\pi} \int_{h}^{H} \frac{dN_L(z)}{dz} \left\{ \int_{h}^{z} \frac{r \, dr}{\left(z^2 - r^2\right)^{\frac{1}{2}} \left(r^2 - h^2 \sin^2 \theta\right)^{\frac{1}{2}}} \right\} dz. \tag{7}$$

The inner integral is available in tables of standard integrals and gives the result

$$N_U(h, \theta) = \frac{1}{\pi} \int_{h}^{H} \frac{dN_L(z)}{dz} \tan^{-1} \left(\frac{z^2 - h^2}{h^2 - d^2}\right)^{\frac{1}{2}} dz. \tag{8}$$

Finally, an integration by parts with $u = \tan^{-1} \left[(z^2 - h^2)/(h^2 - d^2)\right]^{\frac{1}{2}}$ and $dv = \left[dN_L(z)/dz\right] dz$ yields the final transformation as

$$N_U(h, \theta) = \int_{h}^{H} w(h, \theta, z) N_L(z) \, dz \tag{9}$$

where

$$w(h, \theta, z) = \frac{h \cos \theta}{\pi} \frac{z}{\left(z^2 - h^2 \sin^2 \theta\right) \left(z^2 - h^2\right)^{\frac{1}{2}}} \ . \tag{10}$$

9

These two equations comprise the desired transformation. The upsounding radiance profile $N_U(h, \theta)$ is determined directly as a weighted integral over the limb scanning profile $N_L(z)$. Example applications of this transformation are given in Section 4.

The most significant feature of the transformation is that no reference is made to the emission function $J(r)$. If it were necessary for $J(r)$ to be known, it would either have to be calculated or measured. The difficulty of calculating $J(r)$ was discussed briefly in the introduction. Measurement of J can be made by inversion analysis (Gille and House, 1971; Russell and Drayson, 1972). For the optically thin case, (3) is the inversion. An unavoidable aspect of such inversion analysis is the propagation of experimental noise. For example, in (3), even the slightest of random fluctuations (noise fluctuations, not structural variations) in the measured profile of $N_L(z)$ can propagate through the inversion to yield extremely noisy results for $J(r)$. Great care and some form of data smoothing is generally required to perform meaningful inversions. The principal source of noise amplification in the inversion of (3) is the need to consider the derivative of $N_L(z)$. In the transformation procedure considered here, this derivative is eliminated in the final integration by parts leading to (9). [Note: an integration by parts cannot be used to eliminate the derivative in (3)].

The weighting function $w(h, \theta, z)$ is shown in Fig. 3 for two zenith angles. The important feature to note is that the upsounding radiance at altitude h is determined primarily by the magnitude of the limb profile in the vicinity of $z = h$. In fact, as $\theta \rightarrow \pi/2$, $w(h, \theta, z)$ approaches a delta function and yields the obvious result $N_U(h, \pi/2) = \frac{1}{2} N_L(h)$.
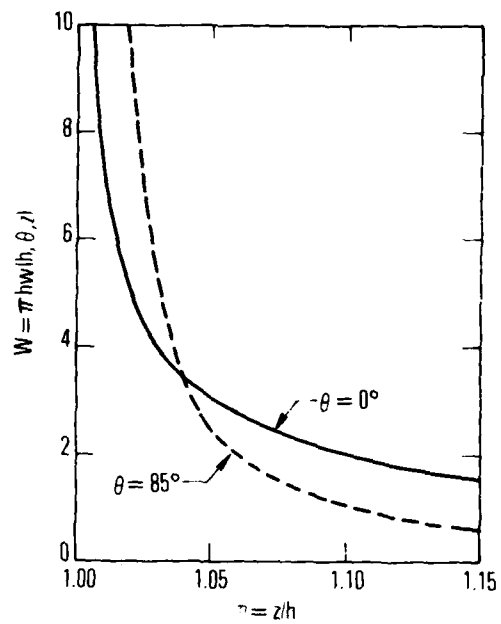
Fig. 3. Transformation Weighting Function

b.   Numerical quadrature

In general, the transformation (9) must be carried out by numerical quadrature. The method used here consists of a simple discretization of the z and h axes into N zones by

$$z, h = z_1, z_2, \ldots, z_{N+1} \tag{11}$$

where $z_1 < z_2 < \ldots < z_{N+1}$, $z_1 = H_0$, and $z_{N+1} = H$ and the assumption that $N_L(z)$ varies linearly between grid points

$$N_L(z) = \alpha_i + \beta_i z$$
$$\alpha_i = N_L(i) - \beta_i z_i \tag{12}$$
$$\beta_i = \frac{N_L(i + 1) - N_L(i)}{\Delta_i}$$

where $\Delta_i = z_{i+1} - z_1$. Substitution of (11) and (12) into (9) yields

$$N_U(j, \theta) = \frac{h \cos \theta}{\pi} \sum_{i=j}^{N} \left\{ \alpha_i F_i + \beta_i G_i \right\} \tag{13}$$

where

$$F_i = \int_{z_i}^{z_{i+1}} \frac{z}{\left(z^2 - h^2 \sin^2 \theta \right) \left(z^2 - h^2 \right)^{\frac{3}{2}}} dz$$

and

$$G_i = \int_{z_i}^{z_{i+1}} \frac{z^2}{\left(z^2 - h^2 \sin^2 \theta \right) \left(z^2 - k^2 \right)^{\frac{3}{2}}} dz.$$

These two integrals can be worked out using tables of standard integrals to give

12

$$F_i = f_{i+1} - f_i$$

where

$$f_i = \frac{1}{h\cos\theta} \tan^{-1}\left\{\frac{\left(z_i^2 - h^2\right)^{\frac{1}{2}}}{h\cos\theta}\right\} \qquad (14)$$

and

$$G_i = g_{i+1} - g_i$$

where

$$g_i = \ell n\left\{z_i \left(z_i^2 - h^2\right)^{\frac{1}{2}}\right\} + \tfrac{1}{2}\tan\theta\left[\sin^{-1}\left\{\frac{h + z_i\sin\theta}{z_i + h\sin\theta}\right\} - \sin^{-1}\left\{\frac{h - z_i\sin\theta}{z_i - h\sin\theta}\right\}\right]. \qquad (15)$$

Substitution of (14) and (15) into (13) and a collection of terms on $N_L(z_i)$ yields the final quadrature formula

$$N_U(j, \theta) = \frac{h\cos\theta}{\pi} \sum_{i=j}^{N+1} \gamma_i N_L(i)$$

where

$$(16)$$

$$\gamma_i = (1 - \delta_{i, N+1})\left\{(f_{i+1} - f_i)\left(1 + \frac{z_i}{\Delta_i}\right) - \frac{(g_{i+1} - g_i)}{\Delta_i}\right\}$$

$$+ (1 - \delta_{i, j})\left\{\frac{(g_i - g_{i-1})}{\Delta_i} - z_{i-1}\frac{(f_i - f_{i-1})}{\Delta_i}\right\}$$

and where $\delta_{nm} = 0$ if $n \neq m$ and $= 1$ if $n = m$.

c. Exponential approximation

In an isothermal, exponential pressure atmosphere with a constant species mixing ratio, the source function is of the form $J(r) \simeq J_0 \exp(-r/\alpha)$ where α is the exponential pressure scale height. Use of this form in (1) gives (with $H \rightarrow \infty$)

$$N_L(z) = 2 J_0 z K_1(z/\alpha) \tag{17}$$

where K_1 is the modified Bessel function of order 1. The argument z/α of K_1 is large (since $z \geq R \simeq 6371\,km$ and $\alpha \sim 7\,km$), and the asymptotic limit of K_1 can be used to obtain

$$N_L(z) \sim J_0 (2\pi\alpha z)^{\frac{1}{2}} e^{-z/\alpha}. \tag{18}$$

The tangent height variation predicted by (18) is very nearly exponential (with the same scale height as J) since the preexponential variation with z is very small within the atmosphere (i.e., $0 \leq z' = z - R \leq 500\,km$). A very nearly exponential fall of $N_L(z)$ above $z - R \simeq 150\,km$ is a common prediction of the Degges model.

If an exponential profile is <u>assumed</u> for $N_L(z)$, then a very simple approximate transformation can be derived from the general transformation of (9). Let

$$N_L(z) = N_0 e^{-z/\alpha'} \tag{19}$$

with $H \to \infty$. Substitution of this profile into (9) and the change of
variable

$$X = \left[\left(\frac{z}{h} \right)^2 - 1 \right]^{\frac{1}{2}} \tag{20}$$

yields

$$N_U(h, \theta) = N_0 \frac{\cos \theta}{\pi} \int_0^\infty \frac{\exp[-(h/\alpha')(1 + X^2)^{\frac{1}{2}}]}{X^2 + \cos^2 \theta} \, dX . \tag{21}$$

For typical α' , $h/\alpha' >> 1$ and the integrand of (21) is very sharply
peaked about $X = 0$. Most of the contribution to the integral will come
from regions where X is small. To a high degree of accuracy, then,
the argument function $\left(1 + X^2 \right)^{\frac{1}{2}}$ may be replaced with $1 + X^2/2$. Doing so,
and evaluating the resulting standard integral yields

$$N_U(h, \theta) \approx \frac{1}{2} N_L(h) \, f(\beta) \tag{22}$$

where

$$f(\beta) = e^{\beta^2} [1 - \mathrm{erf}(\beta)] ,$$

$$\beta \approx \left(\frac{h}{2\alpha'} \right)^{\frac{1}{2}} \cos \theta ,$$

and where (19) has been used to express the final result in terms of $N_L(h)$. Note that the approximation has combined the two independent parameters h and θ into the single parameter β. In the limit $\beta \rightarrow 0$ (e.g., $\theta \rightarrow \pi/2$), $f(\beta) \rightarrow 1$ and $N_U(h) \rightarrow \frac{1}{2} N_L(h)$, which is the correct result. In the limit $\beta \rightarrow \infty$ (e.g., h/α' large and $\theta \rightarrow 0$), $f(\beta) \rightarrow 1/\beta \pi^{\frac{1}{2}}$ and $N_U(h) \rightarrow N_L(h)/[(2\pi h/\alpha')^{\frac{1}{2}} \cos\theta]$.

This approximation is useful even if the limb profile is not exactly exponential, particularly for θ near $\pi/2$. A qualitative measure of the extent of tangent height over which N_L would have to be reasonably exponential in order for the approximation to apply is the half width of the weighting function $\cos\theta/(x^2 + \cos^2\theta)$. This width is $x_{\frac{1}{2}} = \cos\theta$. The corresponding width in z about h is

$$\Delta z \approx h\left(1 + x_{\frac{1}{2}}^2\right)^{\frac{1}{2}} - h$$

$$= h\left[\left(1 + \cos^2\theta\right)^{\frac{1}{2}} - 1\right] . \tag{23}$$

Δz is tabulated in Table 1 for $0 \leq \theta \leq \pi/2$. As θ approaches $\pi/2$, the altitude region over which N_L would have to be exponential in order for the approximation to apply becomes small. The accuracy of the approximation for the worst case of application, that is, $\theta = 0$, is illustrated in Section 4.

16

Table 1. Width Around h Over Which N_L Should Be
Approximately Exponential for Eq. (22)
To Apply.

θ (degrees)	Δz(km)
0	2680
30	2089
60	763
70	368
80	97
85	25
87	9
89	1
90	0

3. Optical Thinness

The transformation of limb data to upsounding data requires the assumption that the atmosphere is optically thin in the sensor bandpass for the lowest tangent height scanned. The most extreme criterion for thinness is that the absorptance over the tangent line of sight at the center of the strongest spectral line in the bandpass be small ($\alpha_C \leq 0.1$ or $\tau_C \geq 0.9$). For a tangent height z, the center line absorptance is

$$\alpha_C = 1 - \exp\left\{ -2 \int_z^\infty c(r)\, p(r)\, k_0(r)\, \frac{r\, dr}{\left(r^2 - z^2\right)^{\frac{1}{2}}} \right\} \qquad (24)$$

where c is mole fraction of active species, p is total atmospheric pressure, and k_0 is the absorption coefficient at the line center, which for a general Voigt line is

$$k_0(r) = \left(\frac{\ln 2}{\pi}\right)^{\frac{1}{2}} \frac{S(r)}{\gamma_D(r)} \quad K_0\left[a(r)\right] \qquad (25)$$

where

$$K_0(a) = e^{a^2}\left[1 - \mathrm{erf}(a)\right], \qquad (26)$$

19

$$a(r) = (\ln 2)^{\frac{1}{2}} \frac{\gamma_L(r)}{\gamma_D(r)} , \tag{27}$$

and

$$\gamma_L(r) = \gamma_0 p(r) . \tag{28}$$

$S(r)$, $\gamma_L(r)$ and $\gamma_D(r)$ are, respectively, the line strength, the pressure broadening (Lorentz) component of the line width, and the Doppler broadening component of the line width. Near the centers of the strong molecular absorption bands, the line strengths are reasonably independent of temperature (and thus of altitude) and we take $S(r) \approx S$. Also assume $c(r) \approx c$ and $\gamma_D(r) \approx \gamma_D$. Then, for an exponential pressure atmosphere

$$p(r) = p_0 e^{-(r-R)/\alpha} \tag{29}$$

with scale height α, the absorptance at tangent height z can be expressed by

$$\alpha_C(\beta) = 1 - \exp\left\{ - 2 c p_0 \left(\frac{\ln 2}{\pi}\right)^{\frac{1}{2}} \frac{S \alpha}{\gamma_D} F(\beta) \right\} \tag{30}$$

where $\beta = z/\alpha$ and

$$F(\beta) = \beta \int_1^\infty e^{-(\beta \rho - \beta_0)} \, K_0 \left\{ a_0 \; e^{-(\beta \rho - \beta_0)} \right\} \frac{\rho \, d\rho}{\left(\rho^2 - 1\right)^{\frac{1}{2}}} \tag{31}$$

with

$$a_0 = (\ell n 2)^{\frac{1}{2}} \frac{\gamma_0 P_0}{\gamma_D} \, ,$$

$\rho = r/z$, and $\beta_0 = R/\alpha$. F was evaluated numerically with $R = 6371$ km, $\alpha = 6.65$ km, $p_0 = 1$ atm, $\gamma_0 = 0.08$ cm^{-1}/atm, and $\gamma_D = 0.0005$ cm^{-1} (thus $a_0 = 133$ and $\beta_0 = 958$). The result is shown in Fig. 4. Also shown is the function $F_D(z)$ that would obtain for a pure Doppler line. This latter case is obtained from (31) in the limit $a_0 \to 0$ and is

$$F_D(\beta) = \beta \int_1^\infty e^{-(\beta \rho - \beta_0)} \frac{\rho \, d\rho}{\left(\rho^2 - 1\right)^{\frac{1}{2}}} = \beta e^{\beta_0} K_1(\beta) \tag{32}$$

where K_1 is the modified Bessel function of order 1. Since β is large ($\beta \geq \beta_0 = 958$), asymptotic limit $K_1(\chi) \sim (\pi/2\chi)^{\frac{1}{2}} e^{-\chi}$ can be used to obtain

$$F_D(\beta) = (\pi\beta/2)^{\frac{1}{2}} e^{-(\beta - \beta_0)} . \tag{33}$$

The comparison in Fig. 4 confirms the well-known result that, for all practical purposes, a purely Doppler line shape can be assumed for altitudes above ~ 50 km.

Equation (30) holds for an isolated line. The most dense crowding of spectral lines occurs in the Q branch of the 15-μm CO_2 band. To a good
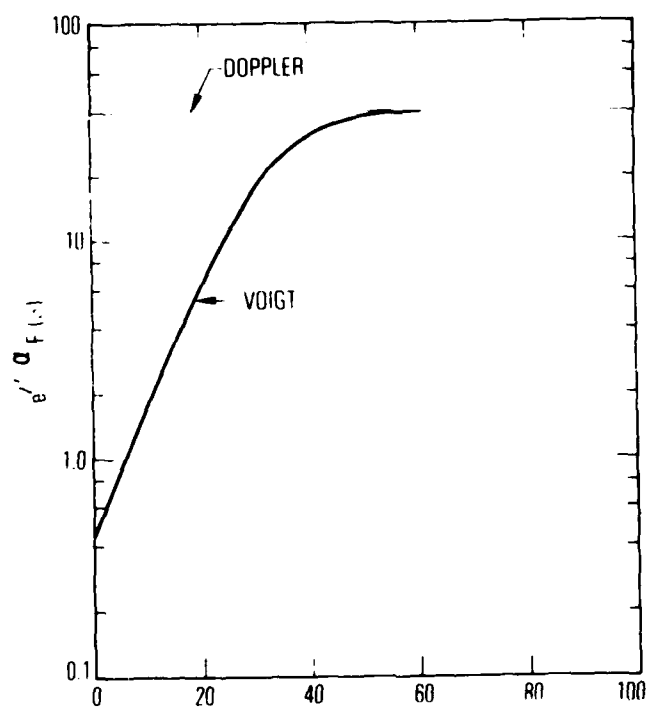
Fig. 4. Line Center Absorptance Function

approximation, the line spacing in the Q branch is given by

$$\delta \simeq (2J + 1)(B' - B'') \tag{34}$$

where J is the rotational quantum number and B' and B'' are the rotational constants of the upper and lower vibrational levels, respectively. The most dense crowding occurs at $J = 0$, and with $B' - B'' = 10.2 \times 10^{-4} \, cm^{-1}$ (Kaplan and Eggers, 1956), (34) yields

$$\delta_{min} \simeq 0.001 \, cm^{-1}.$$

The Doppler line width is $\gamma_D \simeq 0.0005 \, cm^{-1}$ and is half this worst estimate of line spacing. The Lorentz half width is

$$\gamma_L \simeq \gamma_0 \, p_0 \, e^{-(z-R)/\alpha}.$$

With $\gamma_0 = 0.08 \, cm^{-1}$, $p_0 = 1$ atm, and $\alpha = 6.65$ km, the Lorentz width will be smaller than δ_{min} for altitudes $z-R \geqslant 29$ km. Thus, the assumption of isolated lines even in the Q branch is justified for altitudes above ~ 30 km.

The line center absorptance α_C was computed for each of the major absorbing atmospheric species. These species and the locations of their absorption bands are tabulated in Table 2. Within each band, the strongest line was located by searching the AFGL line atlas (McClatchey et al., 1973). This strength and the location ν of the line are also listed in Table II. An estimate of the likely maximum value of species concentration near 100 km altitude is also given in the table (Degges, 1974). From these data, the minimum altitudes for which $\alpha_C \leqslant 0.1$ were computed and are listed in the final column of the table. A plot of $\tau_C = 1 - \alpha_C$ versus $z' = z-R$ for CO_2 is shown in Fig. 5. Except for the CO_2 band, the minimum altitudes are $\sim 100 \pm 10$ km. For CO_2, the altitude is somewhat higher, at about 135 km.

23

Table 2. Maximum Line Strength and Concentration for
Important Atmospheric Absorption Band
(5 to 20 μm)

Species	Band (μm)	S_{max}(cm^{-2}/atm at 296 K)	ν (cm^{-1})	c (mole fraction) at $\simeq$ 100 km	z'_{min}(km)
H_2O	6.3	7.94	1685	3 (-6)	108
CH_4	7.7	1.83	1333	1 (-6)	91
N_2O	7.8	4.36	1298	1 (-6)	101
O_3	9.6	0.99	1053	2 (-6)	91
CO_2	15	7.69	667.7	2 (-4)	136

24
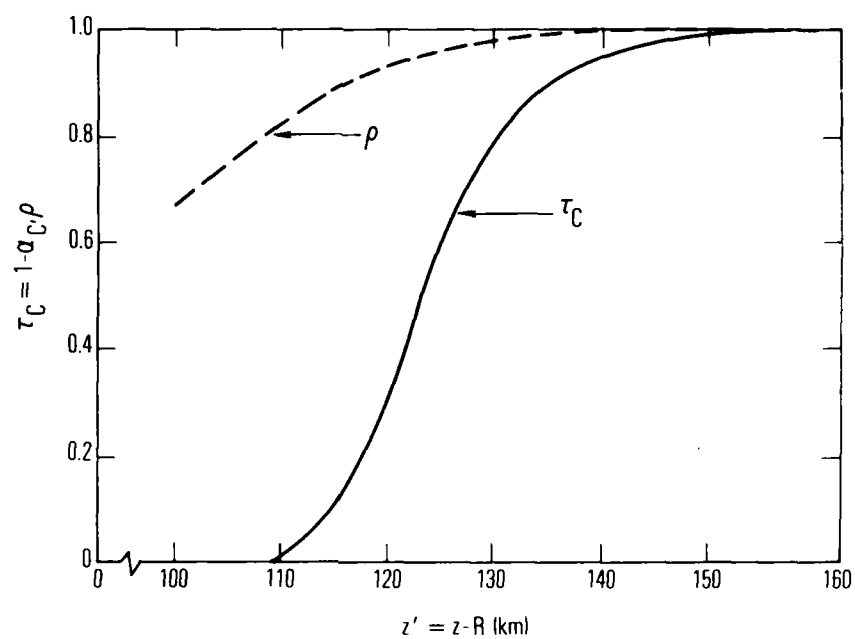
Fig. 5. Line Center Absorptance and Optical Thinness
Parameter ρ for 15-μm CO_2 Band

Because of the number of assumptions made in the derivation of (30) and because of the quality of data (particularly c and α) used, these altitude results should be viewed only as rough upper estimates of the minimum altitude at which optical thinness obtains. For example, results obtained with the Degges code for the 13- to 16-μm CO_2 bandpass (see next section) indicate that optical thinness prevails at lower altitudes. Under optically thin conditions, the "upsounding" radiance at $\theta = \pi/2$ should be exactly half the limb radiance, and the function

$$\rho = \frac{2N_U(z, \pi/2)}{N_L(z)} \qquad (35)$$

should be unity. The function actually deduced from the code calculations is shown in Fig. 5 and displays optical thinness (i.e., $\rho > 0.9$) down to $z' = 115$ km.

In summary, near the centers of strong absorption bands the transformation method should not be applied for tangent heights lower than $z' \sim 100$ km.

4. Example Application

Synthetic limb radiance profiles for $z' \geq 100$ km were generated with the Deggs code for CO_2 in the 13- to 16-μm bandpass and for O_3 in the 9- to 10-μm bandpass. The CO_2 profile is shown in Fig. 6 for both nighttime and daytime conditions. Upsounding profiles for $\theta = 0$, 60, 80 and $90°$ were also computed with the code for the nighttime condition and are shown in Fig. 7. Results of the application of the numerical transformation and the exponential approximation to the night limb profile are shown in Fig. 8 for $\theta = 0°$. Except in the region from 100 to $\sim$130 km, the numerical transform reproduces the model prediction exactly. The discrepancy below 130 km is a result of the violation of the assumption of optical thinness explicit in the formulation of the transformation. For other zenith angles, the agreement between the code and numerical transform predictions is similar. The agreement for $\theta = 0°$ between the code prediction and the exponential profile approximation is essentially exact for altitudes above 300 km. This is to be expected since above this tangent height, the fall-off of the limb profile (Fig. 6) is almost exactly exponential. The error of the approximation is greatest (not counting the error due to the violation of the assumption of optical thinness) at 130 km and amounts to $\sim$16%. The case $\theta = 0°$ is the worst condition of application of the exponential approximation, and the maximum error decreases monotonically to zero as θ goes to $90°$.

Comparisons between code predictions and transformation results for O_3 are shown in Figs. 9-11. The atmosphere is optically thin down to about 90 km in this spectral region, and the agreement between the code prediction and the numerical transformation result is essentially exact for all altitudes and zenith angles (see Fig. 11 for $\theta = 0°$). Below and above the sharp transition in the limb profile (Fig. 9) at 120 km, the exponential approximation is also quite accurate. In the transition region, however, the exponential profile approximation underestimates the upsounding profile by as much as a factor of two.
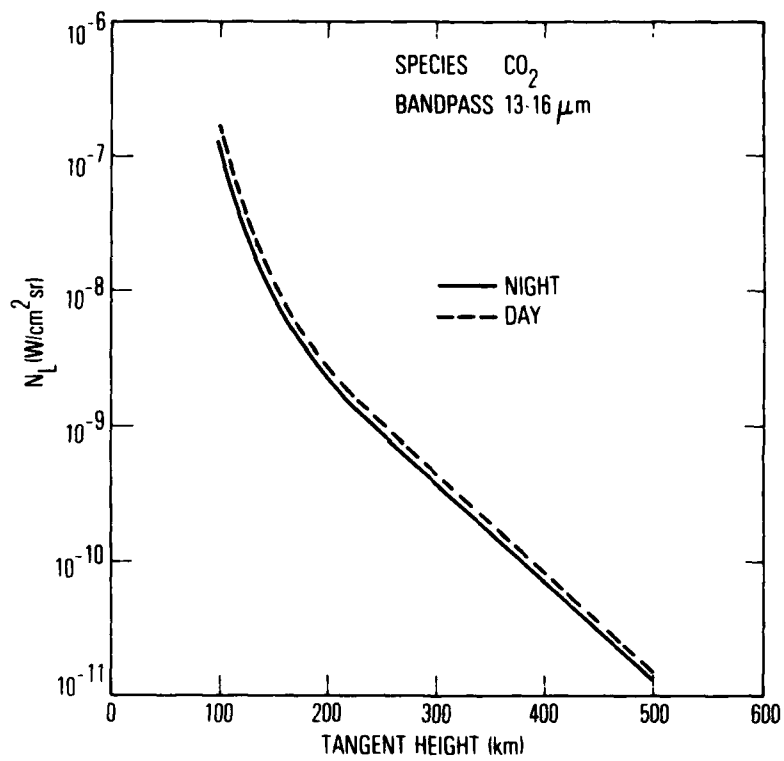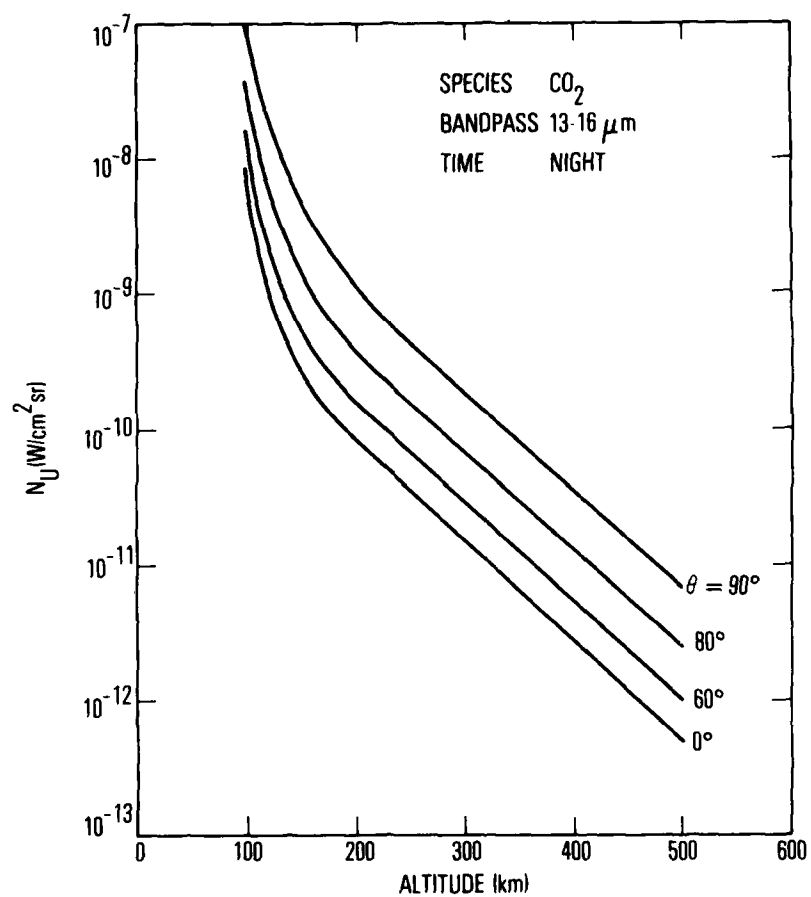
27

Fig. 6. Code Predictions for CO_2 Limb Profiles
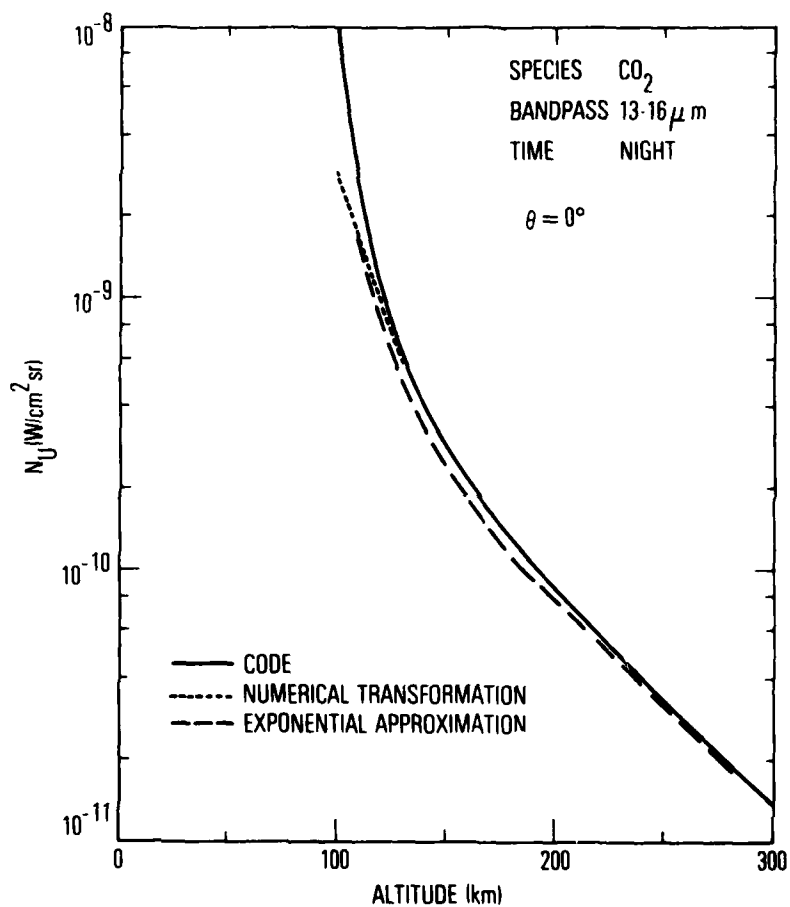
Fig. 7. Code Predictions for CO_2 Upsounding Profiles

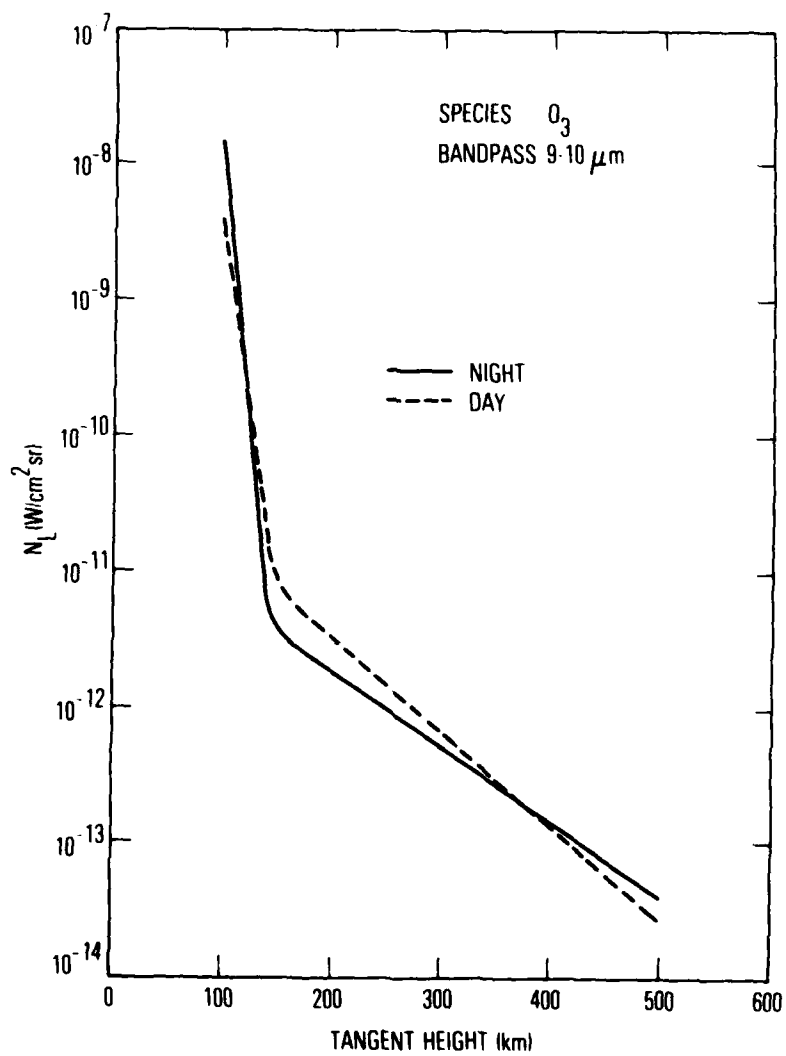Fig. 8. Comparisons Among CO_2 Upsounding Profiles
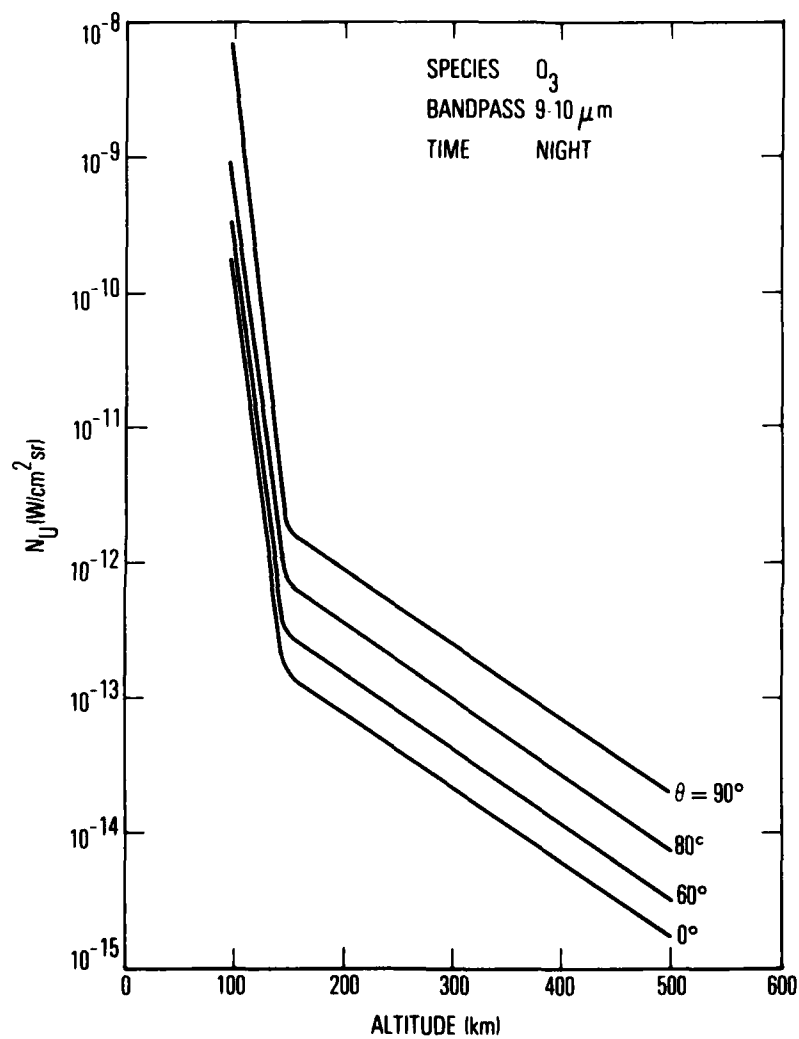
Fig. 9. Code Predictions for O_3 Limb Profiles
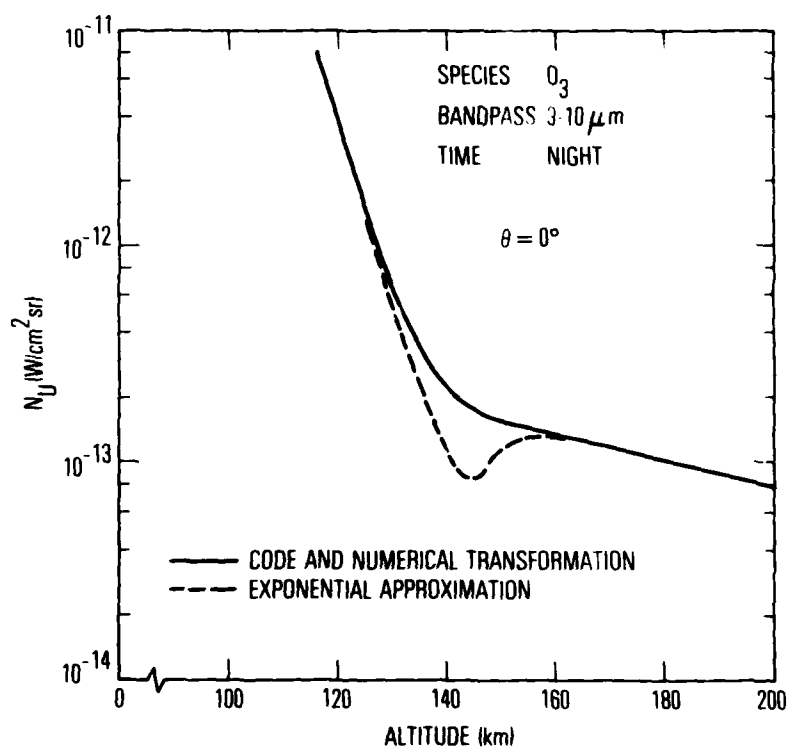
Fig. 10. Code Predictions for O^3 Upsounding Profiles

Fig. 11. Comparisons Among O_3 Upsounding Profiles

References

Degges, T. C., 1974: A high altitude infrared radiance model. AFCRL-TR-0606, Air Force Geophysics Laboratories, Bedford, Mass.

Gille, J. C. and F. B. House, 1971: On the inversion of limb radiance measurements: I. Temperature and thickness. J. Atmos. Sci, 28, 1427-1442.

Kaplan, L. D. and D. F. Eggers, 1956: Intensity and line-width on the 15-micron CO_2 band determined by curve-of-growth method. J. Chem. Phys. 25, 876-883.

McClatchey, R. A., W. S. Benedict, S. A. Clough, D. E. Burch, R. F. Calfe, K. Fox, L. S. Rothman and J. S. Garing, 1973: AFCRL atmospheric absorption line parameter compilation. AFCRL-TR-73-006, Air Force Geophysics Laboratories, Bedford, Mass.

Russell, J. M. and S. R. Drayson, 1972: The inference of atmospheric ozone using satellite horizon measurements of the 1042 cm^{-1} band. J. Atmos. Sci, 29, 376-390.

LABORATORY OPERATIONS

The Laboratory Operations of The Aerospace Corporation is conducting
experimental and theoretical investigations necessary for the evaluation and
application of scientific advances to new military concepts and systems. Ver-
satility and flexibility have been developed to a high degree by the laborato-
ry personnel in dealing with the many problems encountered in the Nation's
rapidly developing space systems. Expertise in the latest scientific develop-
ments is vital to the accomplishment of tasks related to these problems. The
laboratories that contribute to this research are:

Aerophysics Laboratory: Aerodynamics; fluid dynamics; plasmadynamics;
chemical kinetics; engineering mechanics; flight dynamics; heat transfer;
high-power gas lasers, continuous and pulsed, IR, visible, UV; laser physics;
laser resonator optics; laser effects and countermeasures.

Chemistry and Physics Laboratory: Atmospheric reactions and optical back-
grounds; radiative transfer and atmospheric transmission; thermal and state-
specific reaction rates in rocket plumes; chemical thermodynamics and propul-
sion chemistry; laser isotope separation; chemistry and physics of particles;
space environmental and contamination effects on spacecraft materials; lubrica-
tion; surface chemistry of insulators and conductors; cathode materials; sen-
sor materials and sensor optics; applied laser spectroscopy; atomic frequency
standards; pollution and toxic materials monitoring.

Electronics Research Laboratory: Electromagnetic theory and propagation
phenomena; microwave and semiconductor devices and integrated circuits; quan-
tum electronics, lasers, and electro-optics; communication sciences, applied
electronics, superconducting and electronic device physics; millimeter-wave
and far-infrared technology.

Materials Sciences Laboratory: Development of new materials; composite
materials; graphite and ceramics; polymeric materials; weapons effects and
hardened materials; materials for electronic devices; dimensionally stable
materials; chemical and structural analyses; stress corrosion; fatigue of
metals.

Space Sciences Laboratory: Atmospheric and ionospheric physics, radia-
tion from the atmosphere, density and composition of the atmosphere, aurorae
and airglow; magnetospheric physics, cosmic rays, generation and propagation
of plasma waves in the magnetosphere; solar physics, x-ray astronomy; the effects
of nuclear explosions, magnetic storms, and solar activity on the earth's
atmosphere, ionosphere, and magnetosphere; the effects of optical, electromag-
netic, and particulate radiations in space on space systems.

. . .

ATE
LMED
-8